Monolithic CMOS MEMS technology development: A piezoresistive-sensors case study

A. Chaehoi*, D. O'Connell*, D. Weiland*, R. Adamson*, S. Bruckshaw **, S. Ray**, M. Begbie*, J.M. Bruce**

* Institute for System Level Integration, Heriot-Watt Research Park, Research Avenue North, Edinburgh, Scotland, EH14 4AP
Tel: +44 (0)131 510 0670; Fax: +44 (0) 131 449 3141; Aboubacar.Chaehoi@sli-institute.ac.uk
** Semefab Ltd., Newark Road South, Eastfield Industrial Estate, Glenrothes, Scotland, KY7 4NS

ABSTRACT

This paper presents the development of a monolithic CMOS-MEMS platform under the iDesign and SemeMEMS projects with the aim of jointly providing an open access "one-stop-shop" design and prototyping facility for integrated CMOS-MEMS. This work addresses the implementation of a 3-axis accelerometer and a pressure sensor using Semefab's in-house 2-poly 1-metal CMOS process on a 380/4/15μm SOI wafer; the membrane and the proof mass being micromachined using double-sided DRIE. This monolithic approach promises, in high volume production and using low complexity processes, a dramatic cost reduction over hybrid sensors. Furthermore, the embedded signal conditioning and the low-noise level in polysilicon gauges enables high performance to be achieved by implementing dedicated on-chip amplification and filtering circuitry.

Keywords: monolithic, piezoresistive, CMOS, MEMS, inertial, pressure, sensors.

1 INTRODUCTION

Silicon-on-Insulator (SOI) is an attractive material for both VLSI and MEMS sensor applications. While the advantages for the electronics are a reduction in leakage current and parasitic capacitance, bulk etching of the device provides significant seismic mass, thus improving the sensitivity of the sensor by dealing with large forces.
This work addresses the implementation of both a 3-axis accelerometer and an absolute pressure sensor designed by iSLI under the iDesign project and fabricated by Semefab using its in-house MEMS and CMOS technologies on SOI under the SemeMEMS project. The proof mass of the accelerometer is micromachined using Deep Reactive Ion Etching (DRIE) from both sides of the wafer (Fig. 1) and the membrane of the pressure sensor is micromachined using DRIE from one side only. This monolithic approach allows batch production and dramatic cost reduction over hybrid sensors [1] using separate MEMS and signal conditioning circuits. Furthermore, the embedded signal conditioning and in particular, the low noise level in polysilicon gauges enables acceptable performance [2], while the sensitivity is improved by adding dedicated on-chip amplification circuitry. This approach is suitable for applications where highly reliable and low-cost sensors are required [3].

2 SENSOR DEVELOPMENT

The process used for the development of both sensors is a double-poly single-metal CMOS process extended to incorporate double sided DRIE MEMS processing and release, developed by Semefab [4] in collaboration with iSLI [5]. In order to obtain an optimum trade-off between the seismic mass and the stiffness of the beams for the sensors' operating range requirements, a 380/4/15μm SOI wafer was used. Using DRIE to etch the SOI's handle and device layers, and a wet etch of the buried oxide, suspended structures can be obtained as depicted in Fig. 1. For this study, the performance specification required measurement of accelerations up to 300g for the accelerometer and pressures up to 5bar for the pressure sensor.

The micromachined 3-axis accelerometer is composed of four suspended silicon beams attached to a central proof mass. The acceleration is measured by means of polysilicon strain gauges, which convert the stress in the region of the beam anchor points into resistance variations. A reduction in footprint for the piezo-resistive accelerometer is achieved by using the space on the proof mass to site the electronics. This introduces trade-offs in terms of the number and width of tracks to be accommodated on the flexure beams, space for the electronic circuit, space for the attachment of the package and bond pads and the optimum seismic mass available. A two-stage approach using BCB [6, 7] and anodic-bonding was used to package the sensors. The dimensions of the accelerometer's beams are 750×80×15 μm, while the overall fully-packaged accelerometer chip is 3×3×1.9 mm.
The pressure sensor uses the device silicon to form a deformable membrane on which polysilicon strain gauges are deposited with the electronics being laid out on the supporting substrate ring. Initial geometries have been developed and optimized using analytical models and FEM simulations (Fig. 2). The pressure sensor structure contains a 500×500×15 μm membrane with an overall fully-packaged chip size of 1.5×1.3×0.9 mm.

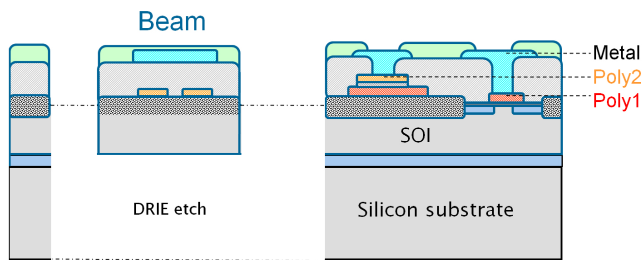

Fig.1: Cross section of the CMOS process on an SOI wafer.

Table 1: Properties of SOI wafer used

Property	Value
Handle-wafer thickness	380 µm
Buried Oxide layer thickness	4 µm
SOI layer thickness	15 µm

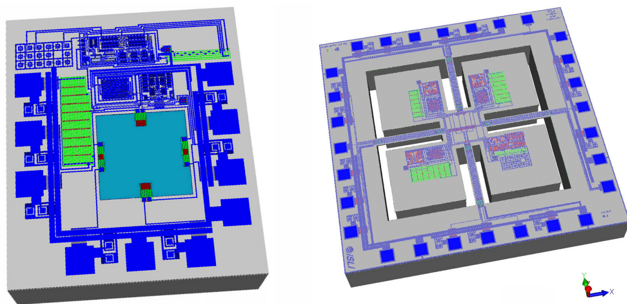

Fig.2: Virtual-prototyping of pressure sensor and accelerometer using CoventorWare®.

3 CONDITIONING ELECTRONICS

The conditioning electronics for the sensors consist of amplifiers (one per axis for the accelerometer and one for the pressure sensor) together with a stable bias generator. Identical amplifiers are used consisting of a differential stage to suit the Wheatstone bridge followed by a common-source stage with the output delivered through a common-drain stage. This gives a large open-loop gain with low output impedance across the anticipated range of transistor parameters. The closed-loop amplifier gain is set by on-chip resistors laid out with the same orientation as the related Wheatstone bridges to assist in process-variation matching. Amplifier gains are set according to the calculated sensitivities above to give a full-scale output of +/-0.5V centered on mid-rail for the target specification of 300g (for in and out of plane channels) and 5bar respectively for the accelerometer and the pressure sensor. To assist with evaluation pin-selectable gain a factor 10 greater than baseline is also available.

Fig. 3 shows the fabricated but unetched accelerometer with one amplifier located in each of three quadrants of the proof mass and the bias generator located in the fourth.

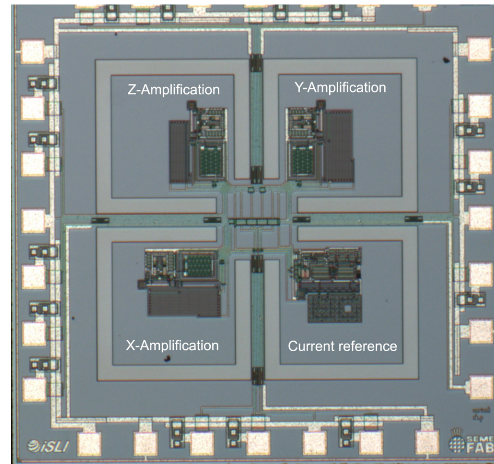

Fig.3: Picture of the integrated 3-axis accelerometer (unetched).

4 SENSOR PERFORMANCE

For this study, the accelerometer performance specifications required accurate acceleration measurement up to 300g. The amplification for the in-plane and out-of-plane axes was designed for a gain of 67 and 40 respectively; an average amplification gain of 63.5 and 38.1 respectively has been measured in test. The input referred noise has been measured at 4.2µV, allowing a resolution of 1.3g over the 3.2kHz bandwidth of the accelerometer.

The pressure sensor specifications required the measurement of pressures up to 5bar. The amplification was designed for a gain of 50 and was measured at 52.6. The pressure sensor exhibits a non-linearity below 1bar (probably due to residual stress in the membrane, among other mechanical effects), this will be the subject of further investigation. Then a very good linearity (less than 2%) is achieved up to 5bar. A sensitivity of 8.7mV/bar is measured in the linear range of the sensor with a resolution of 8mbar over a 540kHz bandwidth.

4.1 Amplifier Gain

The amplifier has two stages each with a gain of around 400. The loop gain is approximately independent of the amplifier/transistor characteristics and defined by the feedback resistor ratio. The gain is a function of the MEMS bridge resistors [R_{bridge}] and the feedback resistor value [$R_{feedback}$]. The designed amplifier gain value [G] assumes a symmetrical differential input signal from the mechanical resistor bridge. This gain value is given by:

$$G = \frac{2R_{feedback}}{R_{bridge}} + 0.5 \quad (1)$$

Equation 1 assumes all bridge resistors are equal. Any variation in either the bridge resistors or the feedback resistor will affect the gain. The bridge resistors and the feedback resistor are made from high resistance poly2 material, having sheet resistance 0.7-1.3 kΩ/sq. Careful design and placement of resistors minimize the effect of variation in sheet resistance across the die and any variation in R_{bridge} will be matched by a corresponding variation in $R_{feedback}$,thus maintaining the amplifier gain. However, variations in bridge resistance values will affect the amplifier gain.

Access to the power-supply of the Wheatstone bridge allows an easy characterization of the amplifier gain and frequency response as shown in Fig. 4.

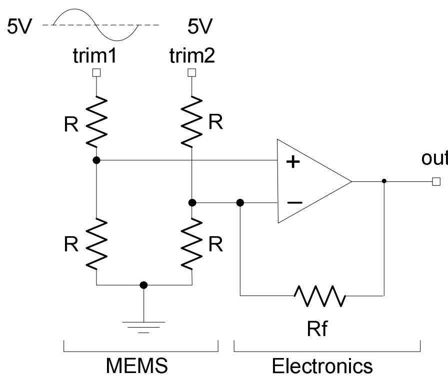

Fig.4: MEMS conditioning circuit.

Fig. 5 shows the simulated and measured Bode plot for the accelerometer in-plane amplifier chain. The Cadence simulation used resistance values derived from measurements. The gain is less than expected. Along with the decrease in gain there is a corresponding increase in bandwidth. The gain bandwidth product (GBW) in the simulated case is 2.95 MHz while the measured GBW is 6 MHz. The larger than designed GBW is due to the fact that the amplifier bias current affects the bandwidth and the bias current is determined in part by a reference resistor made from the highly variable poly2 material.

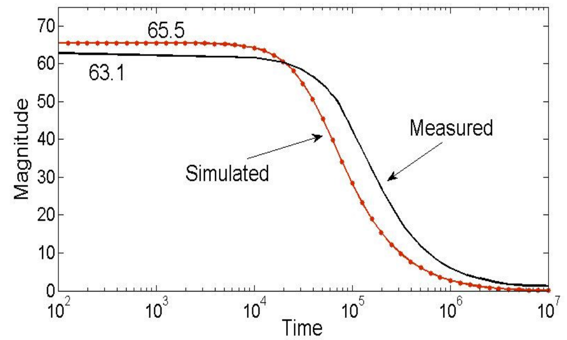

Fig.5: Frequency response of the amplifier.

The amplifier gain was measured at 63.1 and 38.1 respectively for the in-plane and out-of-plane accelerometer amplifier chain, which represents a difference of 3.6% and 5.4% respectively, compared to design. The gain has been measured at 52.6 for the pressure sensor amplifier chain, representing a variation of 3.1% compared to the expected gain. These characterization results closely match the simulation and design specifications.

4.2 Noise

There are two principal noise sources: the thermo-mechanical noise of the structure due to agitation by the surrounding gas; and the electronic noise. Due to the relatively large size of proof mass, the mechanical noise is expected to have a minor influence and can therefore be neglected [8]. Noise measurement was achieved with the following approach. Sampled time domain voltage data, acquired from an oscilloscope, the noise spectral components are then extracted directly by Fourier transform and converted to Vrms using Matlab ®. Analysis of the noise data shows that the measurement set-up adds a considerable amount of 50Hz mains noise to the measurements. A 50Hz bandstop filter was applied to the sampled noise to remove the main noise component. From analysis of the resistor noise contribution it is concluded that the amplifier voltage and current noise are the largest contributors to the noise value. A dedicated board with battery supply was used to provide the lowest noise measurements.

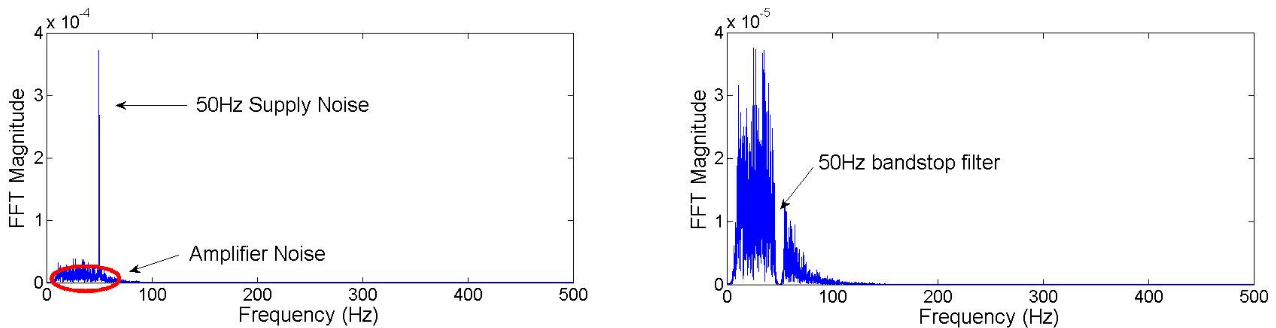

Fig.6: FFT of the noise before and after the 50Hz bandstop filter

Again, an oscilloscope was used to sample the output of the amplifier in the time domain. The scope channel was configured for AC coupling in order to remove the DC component which would give inaccurate rms values. The operating bandwidths of the sensors are up to 3.2kHz and 540kHz, respectively for the accelerometer and the pressure sensor, so the noise data must be sampled at greater than twice this frequency to satisfy Shannon's theorem.
To calculate the rms value of the noise we have converted the sampled noise to the frequency domain and calculated the average power. By measuring the noise at the output of the amplifier and dividing it by the amplifier gain, the input referred noise was calculated as 4.2µVrms.

4.3 Mechanical characterization

Fig. 7 shows the sensitivity response of the pressure sensor. The sensor exhibits a non-linearity below 1bar while a very good linearity is achieved up to 5bar (maximum pressure allowed by our setup). A sensitivity of 8.7mV/bar is measured in the linear range of the sensor when excited with 5V.

Mechanical characterization (shock and vibration) of the accelerometer is currently in progress; therefore the mechanical results are not available yet. However, the modeling and simulation of the sensor predict an intrinsic sensitivity (before amplification) of 53µV/g and 23µV/g, respectively for out-of-plane and in-plane acceleration. From the measured input referred noise and gain, a final sensitivity of 2.02mV/g and 1.46mV/g respectively for out-of-plane and in-plane acceleration and a resolution of 182mg can be expected.

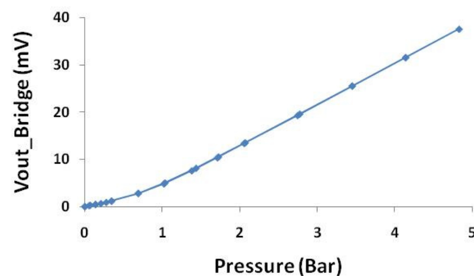

Fig.7: Pressure sensor output vs. applied pressure.

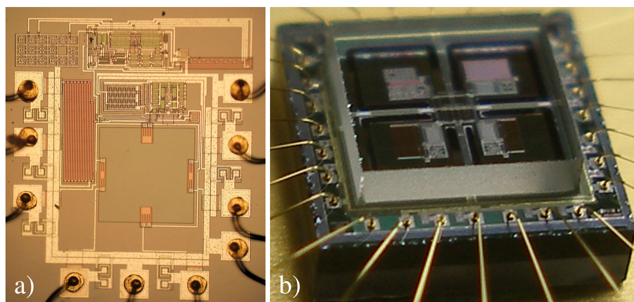

Fig.8: a) Top-view of the absolute pressure sensor
b) Packaged accelerometer with top and bottom Pyrex cap.

5 CONCLUSION

We have presented the successful realization of devices on a new open-access CMOS-MEMS foundry platform for the development of future monolithically integrated MEMS transducers. An absolute pressure sensor and a 3-axis accelerometer developed using this platform have been presented with associated performance data. A complete design-kit – including an electronics library, DRC file, process file, specific material property database [9] and a library of parametric mechanical elements – is under development. This design-kit will facilitate the full design-flow providing third parties an easy and low-risk access to MEMS design and prototyping.

ACKNOWLEDGMENTS

The authors would like to acknowledge the support from the Scottish Higher Education Funding Council through the SCIMPS project. The authors also acknowledge the funding support of Scottish Enterprise and the Technology Strategy Board through the iDesign and the SemeMEMS projects.

REFERENCES

[1] G.K. Fedder, "CMOS-based sensors", Proc. IEEE Sensors Conference, 2005, pp. 125-128.

[2] R. Brederlow, Werner Weber, "Low-frequency noise of integrated polysilicon resistors", IEEE Transactions on Electronics Devices, Vol.48, No.6, pp. 1180-1187, 2001.

[3] S. Renard, "Industrial MEMS on SOI", Journal of Micromechanics and Microengineering Vol.10, pp. 245-249, 2000.

[4] Semefab (Scotland) Ltd., Sensor & Silicon Solutions, www.semefab.co.uk.

[5] Institute for System Level Integration. www.isli.co.uk.

[6] F. Niklaus, H. Andersson, P. Enoksson, G. Stemme, "Low temperature full wafer adhesive bonding of structured wafers", Sensors and Actuators A, 92, pp. 235-241, 2001.

[7] C.H. Wang, J. Zeng, K. Zhao, H.L. Chan, "Chip Scale Studies of BCB Based Polymer Bonding for MEMS Packaging", Proceedings of 2008 Electronic Components and Technology Conference, pp. 1869-1873.

[8] T.B. Gabrielson, "Mechanical-Thermal Noise in Micromachined Acoustic and Vibration Sensors", IEEE Transaction on Electron Devices, Vol. 40, n°5, May 1993.

[9] L. Li, J. Gomes, G. Brown, D. Uttamchandani, W. Pan, D. Weiland, M. Begbie, C. Lowrie, M. Desmulliez, "Simultaneous determination of the Young modulus and Poisson ratio in micro-nano materials", Journal of Micromechanics and Microengineering, 19 (2009).